Acta Mech
DOI 10.1007/s00707-013-0813-6

Vlado A. Lubarda

The shape of a liquid surface in a uniformly rotating cylinder in the presence of surface tension

Received: 25 September 2012 / Revised: 24 December 2012

Abstract The free-surface shape of a liquid in a uniformly rotating cylinder in the presence of surface tension is determined before and after the onset of dewetting at the bottom of the cylinder. Two scenarios of liquid withdrawal from the bottom are considered, with and without deposition of thin film behind the liquid. The governing non-linear differential equations for the axisymmetric liquid shapes are solved numerically by an iterative procedure similar to that used to determine the equilibrium shape of a liquid drop deposited on a solid substrate. The numerical results presented are for cylinders with comparable radii to the capillary length of liquid in the gravitational or reduced gravitational fields. The capillary effects are particularly pronounced for hydrophobic surfaces, which oppose the rotation-induced lifting of the liquid and intensify dewetting at the bottom surface of the cylinder. The free-surface shape is then analyzed under zero gravity conditions. A closed-form solution is obtained in the rotation range before the onset of dewetting, while an iterative scheme is applied to determine the liquid shape after the onset of dewetting. A variety of shapes, corresponding to different contact angles and speeds of rotation, are calculated and discussed.

1 Introduction

The mechanics of rotating fluids is an important part of the analysis of numerous scientific and engineering problems. These include the problems from earth and planetary science, stability analysis of projectiles and satellites with spinning fluid tanks, atmospheric and oceanic circulation, turbomachinery, centrifuges, liquid handling and fluid management systems, rotating liquid metals, liquid mirrors, liquid nuclei, etc. [1–4]. The present paper is devoted to the analysis and numerical determination of the gyrostatic shape of a liquid in a rotating cylinder in the presence of surface tension and gravity. There has been a considerable interest devoted to this problem in the past, because of its importance for centrifugal casting of optical surfaces, such as mirrors and contact lenses, and for exploring the effects of microgravity on fluids [5–14]. The study is related to other problems of rotating liquid masses, which include the determination of gyrostatic shapes of rotating drops held together by surface tension, rotating liquid bridges between flat plates, liquid rings around solid rods, rotating pendant drops and liquid columns, liquid in eccentric grooves on a rotating disk, and other rotating systems

V. A. Lubarda (✉)
Department of Mechanical and Aerospace Engineering, University of California,
San Diego La Jolla, CA 92093-0411, USA
E-mail: vlubarda@ucsd.edu
Tel.: +1-858-5343169
Fax: +1-858-5345698

V. A. Lubarda
Montenegrin Academy of Sciences and Arts, R. Stijovića 5,
81000 Podgorica, Montenegro

Published online: 02 February 2013

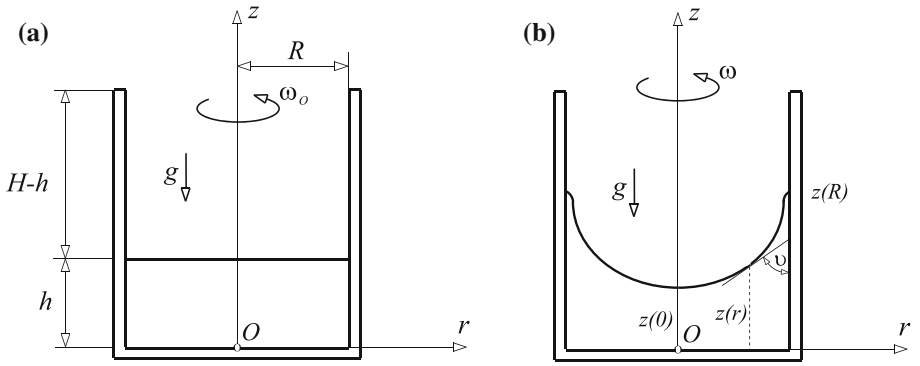

Fig. 1 **a** An imagined reference configuration of liquid in a rotating circular cylinder of inner radius R and height H. The height of the still liquid before its rise and without the capillary effects is h. **b** An axisymmetric shape of the liquid surface under uniform rotation with the angular speed ω, and the same angular momentum as in part (**a**)

in which the meniscus profile does not intersect the axis of rotation [15–18]. There are many other problems in fluid mechanics in which capillary effects play an important role. For example, the influence of the contact angle between a thin fluid film and side walls of an inclined open channel on the velocity profile and instability of the free surface have been recently studied analytically and experimentally in [19,20]. Various problems of liquid dynamics and sloshing in spinning tanks are discussed in [4], which also offers a comprehensive list of references in this field.

2 Liquid shape in a rotating cylinder before dewetting

Figure 1a shows an imagined reference configuration of the system, just upon the removal of external torque, which brought the system to a rotating state. The reference configuration is virtual in the sense that it is assumed that liquid has not yet begun to rise from its still level (h) and that capillary effects are frozen. The moment of inertia of the liquid in this state is $J_0 = mR^2/2$, the moment of inertia of the rigid cylinder is $J_\bullet$, and $\omega_0 = \mathcal{H}/(J_0 + J_\bullet)$ is the angular speed corresponding to a given angular momentum $\mathcal{H}$. The mass of the liquid is $m = \rho_l V$, where ρ_l as its density. The volume of the liquid is $V = \pi R^2 h$, and R is the internal radius of the cylinder. The internal energy associated with this virtual liquid configuration, up to a constant term, is

$$U_0 = R^2\pi\sigma_{lv} + 2\pi Rh\sigma_{sl} + 2\pi R(H-h)\sigma_{sv} + 2\pi R\tau + \frac{1}{2}\gamma_l\pi R^2h^2. \tag{2.1}$$

The height of cylinder's wall is H, and $\gamma_l = \rho_l g$ is the specific weight of the liquid, where g denotes the acceleration of the gravity. The density of the surrounding gas is assumed to be much smaller than the density of the liquid ($\rho_v \ll \rho_l$); otherwise, the specific weight difference $\Delta\gamma = \gamma_l - \gamma_v$ should appear in place of γ_l in the last term on the right-hand side of (2.1). The solid/vapor and liquid/vapor surface energies are denoted by σ_{sv} and σ_{lv}, the solid/liquid interface energy is σ_{sl}, and τ is the line tension along the triple solid/liquid/vapor contact line. The kinetic energy of the liquid in this configuration is $K_0 = (1/2)J_0\omega_0^2$.

After removal of the external torque by which the cylinder was set in rotation, and upon the transient time and decay of viscous oscillations,[1] the liquid is in a state of rigid rotation around the z axis (Fig. 1b), with the angular velocity corresponding to a given angular momentum $\mathcal{H} = (J_0 + J_\bullet)\omega_0 = (J + J_\bullet)\omega$. Assuming that the shape of the liquid surface is axisymmetric and described by a single-valued function $z = z(r)$, the internal energy of the system, up to a constant term, is

$$U = \sigma_{lv}S + 2\pi Rz(R)(\sigma_{sl} - \sigma_{sv}) + 2\pi R\tau + \gamma_l\int_0^R \pi r z^2\,\mathrm{d}r. \tag{2.2}$$

[1] The manner in which the state of rigid rotation of the liquid contained in the cylinder is established (i.e., the development of the Ekman layer, the inviscid fluid spin-up, and the viscous decay of residual oscillations) is not discussed in this paper, but has been studied in the past [21–23]. In a sense, an inverse problem of centrifugal instabilities during spin-down to rest of a viscous incompressible fluid in a rigid cylindrical container, brought to rest impulsively, has been studied in [24]. Additional references can be found in [4].

We neglect the small effect of gravity and angular speed on the surface energy σ_{lv}. The corresponding kinetic energy of the liquid is

$$K = \frac{1}{2} J\omega^2, \quad J = 2\pi\rho_l \int_0^R r^3 z \, \mathrm{d}r. \tag{2.3}$$

The area S in (2.2) is the surface area of the liquid/vapor interface, whose profile $z = z(r)$ is to be determined. The expressions for the surface area S and the volume V are

$$S = 2\pi \int_0^R r(1 + z'^2)^{1/2} \, \mathrm{d}r, \quad V = 2\pi \int_0^R rz \, \mathrm{d}r. \tag{2.4}$$

It is assumed that the angular velocity is sufficiently small so that the surface of the liquid does not touch the bottom of the cylindrical container, so that the interface energy $\pi R^2 \sigma_{sl}$ is the same in the configurations (a) and (b) of Fig. 1, and thus excluded from expressions (2.1) and (2.2). The extension of the analysis to include the withdrawal of liquid from the bottom of the cylinder (dewetting) will be presented in Sect. 3.

The effective mechanical potential of the system is $L = U - K$. If it is assumed that there is no fluid evaporation, the appropriate functional for the variational study is $\Pi = L - \lambda V$, where λ is the Lagrangian multiplier, with the dimension of pressure. It is also assumed that the height H of the cylinder is large enough so that liquid does not spill over the side of the cylinder. In view of (2.1)–(2.4), the potential Π can be written as

$$\Pi = \int_0^R \Phi(r, z, z') \, \mathrm{d}r, \tag{2.5}$$

where, to within a constant term,

$$\Phi = 2\pi \left\{ \sigma_{lv} r \left(1 + z'^2\right)^{1/2} + rz \left[\frac{1}{2} \gamma_l \left(z - \frac{\omega^2}{g} r^2 \right) - \lambda \right] + (\sigma_{sl} - \sigma_{sv}) z \, \bar{\delta}(R - r) \right\}. \tag{2.6}$$

The Dirac delta function is denoted by $\bar{\delta}$.

The variation of Π, corresponding to the variation δz of the shape of the surface S, is

$$\delta\Pi = \int_0^R \left[\frac{\partial \Phi}{\partial z} \delta z + \frac{\partial \Phi}{\partial z'} \frac{\mathrm{d}}{\mathrm{d}r} (\delta z) \right] \mathrm{d}r. \tag{2.7}$$

Upon integration by parts of the second term on the right-hand side of (2.7), this becomes

$$\delta\Pi = \int_0^R \left[\frac{\partial \Phi}{\partial z} - \frac{\mathrm{d}}{\mathrm{d}r} \left(\frac{\partial \Phi}{\partial z'} \right) \right] \delta z \, \mathrm{d}r + \left(\frac{\partial \Phi}{\partial z'} \delta z \right)_{r=0}^{r=R}. \tag{2.8}$$

By dividing (2.8) with the variation $\delta z(\varrho)$ at an arbitrary $\varrho \in [0, R]$, we obtain

$$\frac{\delta\Pi}{\delta z(\varrho)} = R \left[\frac{\partial \Phi}{\partial z} - \frac{\mathrm{d}}{\mathrm{d}r} \left(\frac{\partial \Phi}{\partial z'} \right) \right]_{r=\varrho} + \left[\frac{\partial \Phi}{\partial z'} \bar{\delta}(r - \varrho) \right]_{r=0}^{r=R}. \tag{2.9}$$

The first term on the right-hand side has the usual form of the Euler–Lagrange's equation of the variational principle, while the second term accounts for the boundary conditions. Consequently, upon evaluating the gradients of Φ from (2.6), there follows

$$\begin{aligned} \frac{\delta\Pi}{\delta z(\varrho)} = {} & 2\pi R\varrho \left\{ -2\sigma_{lv}\kappa(\varrho) + \gamma_l \left[z(\varrho) - \frac{\omega^2}{2g} \varrho^2 \right] - \lambda \right\} \\ & + 2\pi R(\sigma_{sl} - \sigma_{sv} + \sigma_{lv} \cos\theta) \, \bar{\delta}(R - \varrho). \end{aligned} \tag{2.10}$$

The mean curvature of the liquid's profile is

$$\kappa(r) = \frac{1}{2}\left[\frac{z'}{r(1+z'^2)^{1/2}} + \frac{z''}{(1+z'^2)^{3/2}}\right], \tag{2.11}$$

while the cosine of the angle between the tangent to the surface profile and the vertical wall of the cylinder is $\cos\theta = z'(R)/[1+z'^2(R)]^{1/2}$.

2.1 Equilibrium conditions

In the gyrostatic configuration, the potential Π has a stationary value, and the expression in (2.10) must vanish. This gives

$$2\sigma_{lv}\kappa(\varrho) - \gamma_l\left[z(\varrho) - \frac{\omega^2}{2g}\varrho^2\right] + \lambda = 0, \tag{2.12}$$

$$\sigma_{sl} - \sigma_{sv} + \sigma_{lv}\cos\theta = 0. \tag{2.13}$$

The term $2\sigma_{lv}\kappa(r)$ represents the projection of the surface tension σ_{lv}, acting along the circumference of an infinitesimal surface element $\mathrm{d}S$, onto the outward direction orthogonal to $\mathrm{d}S$. Consequently, the remaining terms on the left-hand side of (2.12) represent the pressure difference $\Delta p(r) = p_v(r) - p_l(r)$ across the vapor/liquid interface, so that

$$2\sigma_{lv}\kappa(r) - \Delta p(r) = 0, \quad \Delta p(r) = \gamma_l\left[z(r) - \frac{\omega^2}{2g}r^2\right] - \lambda. \tag{2.14}$$

The term $(\rho_l\omega^2 r^2/2)$ is the rotation-induced dynamic pressure. From (2.14), by taking $r = 0$, the Lagrangian multiplier λ can be given the interpretation $\lambda = \gamma_l z(0) - \Delta p(0)$. Consequently, the differential equation for the shape of the liquid/vapor interface becomes

$$\kappa(r) = \frac{\gamma_l}{2\sigma_{lv}}\left[z(r) - z(0) - \frac{\omega^2}{2g}r^2\right] + \frac{\Delta p(0)}{2\sigma_{lv}}. \tag{2.15}$$

In particular, the curvature at the bottom is $\kappa(0) = \Delta p(0)/(2\sigma_{lv})$, so that (2.15) can be rewritten as

$$\kappa(r) = \kappa(0) + \frac{\gamma_l}{2\sigma_{lv}}\left[z(r) - z(0) - \frac{\omega^2}{2g}r^2\right]. \tag{2.16}$$

This equation is analogous to the Young–Laplace differential equation describing the shape of a liquid drop deposited on a smooth solid substrate, apart from the presence of the rotation-induced dynamic pressure term on its right-hand side [25,26].

The second equilibrium condition (2.13) yields the Young's equation for the contact angle,

$$\cos\theta = \frac{\sigma_{sv} - \sigma_{sl}}{\sigma_{lv}}, \tag{2.17}$$

independently of g and ω. The angle θ does not decrease with the increasing angular velocity, as it does in the absence of surface tension, because it is a local material property, governed by the surface tensions alone, unaffected by the external fields due to gravity and rotation. The independence of the equilibrium contact angle of gravity is well known in the mechanics of liquid drops deposited on a flat solid substrate [27–29].

2.2 Stability of equilibrium

The axisymmetric gyrostatic configuration of a rigidly rotating liquid in a cylindrical container, before the onset of dewetting, is unique and stable. The first variation of the potential Π in (2.5) is given by (2.7). Its second variation is

$$\delta^2\Pi = \int_0^R \left[\frac{\partial^2\Phi}{\partial z^2}(\delta z)^2 + 2\frac{\partial^2\Phi}{\partial z\partial z'}\delta z\delta z' + \frac{\partial^2\Phi}{\partial z'^2}(\delta z')^2\right]\mathrm{d}r, \tag{2.18}$$

i.e.,

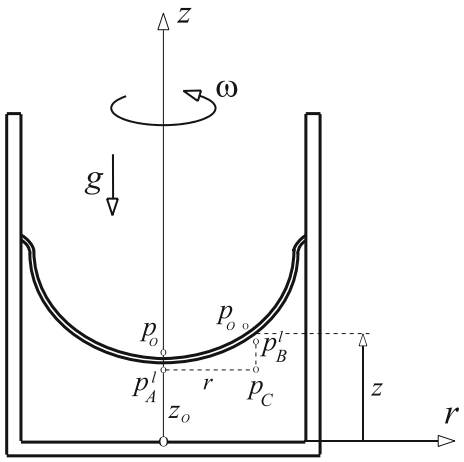

Fig. 2 The liquid pressure at point C can be calculated from the liquid pressures at points A and B. The pressure jumps across the liquid/vapor interface at points A and B can be expressed in terms of local curvatures by the Young–Laplace equation

$$\delta^2\Pi = \int_0^R \left[\rho_l g(\delta z)^2 + \frac{\sigma_{lv}}{(1+z'^2)^{3/2}}(\delta z')^2\right] 2\pi r \, \mathrm{d}r. \tag{2.19}$$

Since the surface tension σ_{lv} is positive, from (2.19) it follows that, for $g \geq 0$, the second variation of the potential Π is everywhere positive ($\delta^2\Pi > 0$), so that the potential Π is a convex functional in the entire space of single-valued functions $z = z(r)$ for the liquid shape. It can be shown that it is also convex in the space of non-axisymmetric single-valued functions $z = z(x, y)$; see [2], p. 157. Consequently, the gyrostatic configuration determined from the stationarity condition $\delta\Pi = 0$ corresponds to the minimum of Π and represents unique and stable gyrostatic configuration. The uniqueness of the shape of capillary surface in the case of a non-rotating circular cylinder has been previously proven in [30,31]. The non-uniqueness does occur in problems with the opposite direction of gravity and in the absence of lateral constraint, for example, rotating pendant drops and liquid bridges between flat plates, which can develop a longitudinal (amphora mode) instability, or a skipping-rope (C-mode) instability; see [2,16], and the references therein.

2.3 Direct derivation of the governing ODE

A simple direct derivation of the governing differential Eq. (2.16) is as follows. The liquid pressure p_C at point C in Fig. 2 can be calculated from the liquid pressure at either the point A or B (p_A^l or p_B^l), by adding the dynamic or hydrostatic pressure contribution, respectively. This gives $p_C = p_A^l + \rho_l(r\omega)^2/2$ and $p_C = p_B^l + \gamma_l(z - z_0)$. Thus,

$$p_A^l - p_B^l = \gamma_l(z - z_0) - \frac{1}{2}\rho_l r^2\omega^2. \tag{2.20}$$

On the other hand, by the Young–Laplace equation, the pressure discontinuities across the liquid/vapor interface at the points A and B are $p_0 - p_A^l = 2\sigma_{lv}\kappa(0)$ and $p_0 - p_B^l = 2\sigma_{lv}\kappa(r)$, so that

$$p_A^l - p_B^l = 2\sigma_{lv}[\kappa(r) - \kappa(0)]. \tag{2.21}$$

By equating (2.20) and (2.21), there follows (2.16). While this derivation is appealing, the derivation based on the variational approach is more general, because it also delivers the expression for the contact angle θ, confirming the validity of Young's Eq. (2.17) in the presence of gravity and centrifugal force.

2.4 Numerical integration

The integration of the differential Eq. (2.16) proceeds as follows. In view of the identity

$$\frac{\mathrm{d}}{\mathrm{d}r}\left[\frac{rz'}{(1+z'^2)^{1/2}}\right]=\frac{rz''}{(1+z'^2)^{3/2}}+\frac{z'}{(1+z'^2)^{1/2}}, \tag{2.22}$$

Eq.(2.16) can be rewritten as

$$\frac{\mathrm{d}}{\mathrm{d}r}\left[\frac{rz'}{(1+z'^2)^{1/2}}\right]=2\kappa(0)r+\frac{\gamma_l}{\sigma_{lv}}\left[rz-rz(0)-\frac{\omega^2}{2g}r^3\right]. \tag{2.23}$$

Since $z'(0)=0$, the integration of (2.23) gives

$$\cos\theta=\frac{z'}{(1+z'^2)^{1/2}}=\kappa(0)r+\frac{\gamma_l}{\sigma_{lv}}\left[\frac{1}{r}\int_0^r\varrho z(\varrho)\,\mathrm{d}\varrho-\frac{1}{2}rz(0)-\frac{\omega^2}{8g}r^3\right]. \tag{2.24}$$

At $r=R$, (2.24) gives

$$2\kappa(0)-\frac{\gamma_l}{\sigma_{lv}}z(0)=\frac{2\cos\theta}{R}-\frac{\gamma_l}{\sigma_{lv}}\left(\frac{V}{\pi R^2}-\frac{\omega^2}{4g}R^2\right). \tag{2.25}$$

By substituting (2.25) into (2.16), there follows

$$\frac{z''}{(1+z'^2)^{3/2}}+\frac{z'}{r(1+z'^2)^{1/2}}-\frac{\gamma_l}{\sigma_{lv}}z=\frac{2\cos\theta}{R}-\frac{\gamma_l}{\sigma_{lv}}\left[h-\frac{\omega^2}{4g}(R^2-2r^2)\right]. \tag{2.26}$$

The accompanying boundary conditions are

$$z(0)=z_0,\quad z'(0)=0,\quad z'(R)=\cot\theta=\frac{\sigma_{sv}-\sigma_{sl}}{[\sigma_{lv}^2+(\sigma_{sv}-\sigma_{sl})^2]^{1/2}}. \tag{2.27}$$

The constant volume condition provides an implicit expression for z_0, such that

$$2\int_0^R rz(r)\,\mathrm{d}r=R^2h. \tag{2.28}$$

The non-dimensional form of (2.26) is

$$\frac{\bar{z}''}{(1+\bar{z}'^2)^{3/2}}+\frac{\bar{z}'}{\bar{r}(1+\bar{z}'^2)^{1/2}}-Bo\,\bar{z}=2\cos\theta-Bo\left[\bar{h}-\frac{\eta}{4}(1-2\bar{r}^2)\right], \tag{2.29}$$

where $\bar{r}=r/R$, $\bar{z}=z/R$, and $\bar{h}=h/R$. The Bond number is

$$Bo=\left(\frac{R}{l_o}\right)^2=\frac{R^2\rho_l g}{\sigma_{lv}}\quad l_o^2=\frac{\sigma_{lv}}{\rho_l g}, \tag{2.30}$$

where l_o is the capillary length [40], while the non-dimensional number $\eta=R\omega^2/g$ represents the ratio of the maximum centrifugal and gravity accelerations. By introducing the rotation-induced capillary length l_ω, and the associated rotation-induced Bond number [15]

$$B_\omega=\left(\frac{R}{l_\omega}\right)^2=\frac{\rho_l R^3\omega^2}{\sigma_{lv}},\quad l_\omega^2=\frac{\sigma_{lv}}{\rho_l R\omega^2}, \tag{2.31}$$

the comparison of (2.30) and (2.31) establishes the connection

$$\eta=\frac{B_\omega}{Bo}=\left(\frac{l_o}{l_\omega}\right)^2=\frac{R\omega^2}{g}. \tag{2.32}$$

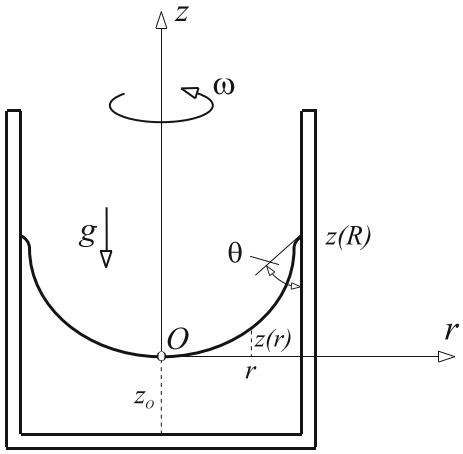

Fig. 3 The coordinate origin placed at the lowest point of the liquid surface. The depth of liquid below the coordinate origin is z_0

2.5 Numerical results

In the numerical treatment, it is convenient to place the coordinate origin at the bottom point of the liquid/vapor interface (Fig. 3), and use the following iterative procedure, similar to the well-known procedure used to determine the equilibrium shape of a liquid drop deposited in the gravity field on a solid substrate [32–35]. Other methods of integration are possible [36]. For given θ, Bo, and η, one assumes the value for $\bar{h}$ and solves (2.29), subject to the boundary conditions $\bar{z}(0) = 0$ and $\bar{z}'(0) = 0$. If the resulting slope $\bar{z}'(1) \neq \cot\theta$, the value of $\bar{h}$ is modified until $\bar{z}'(1) = \cot\theta$. Denote the so-determined $\bar{h}$ by $\bar{h}_0$. If the actual (normalized) initial height of the liquid is $\bar{h} > \bar{h}_0$, there is a cylindrical portion of the liquid below the lowest point of the liquid surface, whose height is $z_0 = (\bar{h} - \bar{h}_0)R$. There are infinitely many solutions of Eq. (2.29), but only those profiles that actually touch or intersect the vertical wall $r = R$ are of interest, and only one of them corresponds to a given contact angle between the liquid and the wall, and a given volume of the liquid. On the other hand, if $\bar{h} < \bar{h}_0$, dewetting takes place, which will be analyzed in Sect. 3.

Figure 4a, b shows the liquid surface shape in the case $\theta = 45°$ and 135°, corresponding to Bond's number $Bo = 50$, and $\eta = 5\,(B_\omega = 250)$. The dashed curves specify the liquid shape in the case when the surface tension effects are ignored, calculated from the expressions listed in the Appendix of the paper. In both cases, the normalized volume of liquid, defined as $\bar{V} = V/(\pi R^3) \equiv \bar{h}$, was equal to $\bar{V} \approx 1.14365$, as obtained by the described iterative procedure of solving (2.29). Without the surface tension effects, dewetting takes place up to the radius $\bar{R}_0 = 0.2085$, with the maximum elevation of the surface $\bar{z}(R) = 2.3913$.

Figure 4c–f shows the increasing effect of the surface tension with the decrease of the Bond number (i.e., the decrease of the radius R relative to the liquid capillary length l). A particularly pronounced effect is seen in Fig. 4f, which corresponds to the hydrophobic surface of the cylindrical wall and the contact angle $\theta = 135°$. The liquid volume was $\bar{V} = 0.42351$. The hydrophobicity is such that the surface tension suppresses the liquid rising above the liquid elevation at the center of the cylinder, so that in this case the liquid shape is almost cylindrical. The volumes in each case are chosen so that the liquid surface just touches the bottom of the cylinder at its center (solid curves in Fig. 4a, c, and e, with the included surface tension effect).

3 Dewetting of the bottom surface of the cylinder

For a sufficiently high angular speed, the bottom of the meniscus surface will approach the bottom of the cylinder to a distance of the order of liquid's molecular size, that is, touch the bottom of the cylinder at the continuum-level modeling. Denote the corresponding angular speed, at which $z(0) = 0$, by ω_*. From Eq. (2.25), there follows

$$R\kappa_*(0) = \cos\theta + \frac{1}{8}\,B_{\omega_*} - \frac{1}{2}\,B_o\bar{h}, \quad B_{\omega_*} = \frac{R^3\rho_l\omega_*^2}{\sigma_{lv}}. \tag{3.1}$$

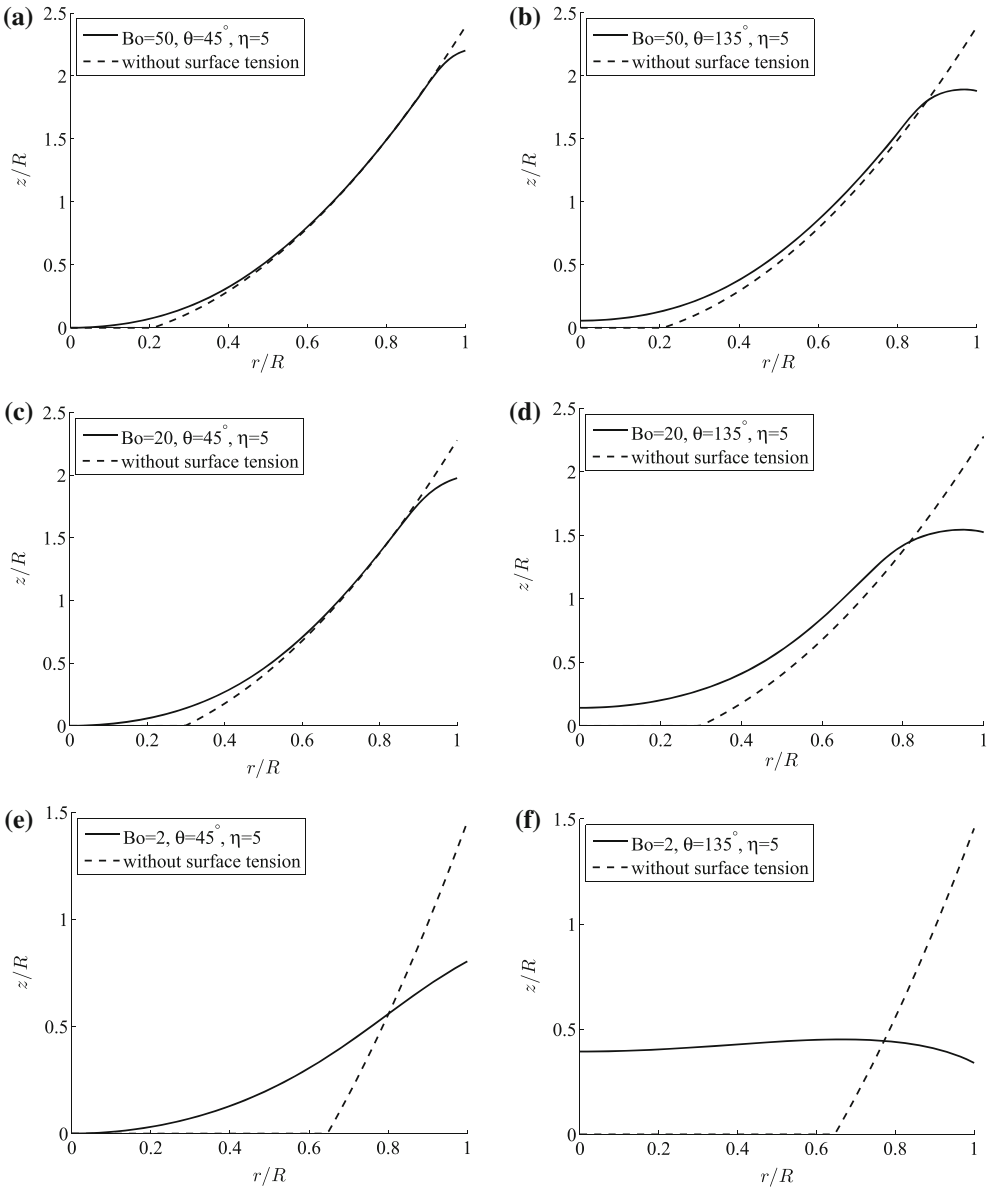

Fig. 4 The shape of the liquid surface, corresponding to the indicated values of Bo, η, and θ. In parts **a** and **b**, the normalized liquid volume is $\bar{V} \approx 1.14365$. Without the surface effects, $\bar{R}_0 = 0.2085, \bar{z}(R) = 2.3913$. With the surface effects: **a** $\bar{z}(0) = 0, \bar{z}(R) = 2.2011$, and **b** $\bar{z}(0) = 0.0565, \bar{z}(R) = 1.8231$. In parts **c** and **d**, the normalized liquid volume is $\bar{V} \approx 1.03738$. Without the surface effects, $\bar{R}_0 = 0.2983, \bar{z}(R) = 2.2775$. With the surface effects: **c** $\bar{z}(0) = 0, \bar{z}(R) = 1.9761$, and **d** $\bar{z}(0) = 0.1416, \bar{z}(R) = 1.5229$. In parts **e** and **f**, the normalized liquid volume is $\bar{V} \approx 0.42351$. Without the surface effects, $\bar{R}_0 = 0.6465, \bar{z}(R) = 1.4552$. With the surface effects: **e** $\bar{z}(0) = 0, \bar{z}(R) = 0.8035$, and **f** $\bar{z}(0) = 0.3938, \bar{z}(R) = 0.3398$

For a known θ, this equation specifies the radius of the curvature at the bottom of the meniscus at the instant of its touchdown with the bottom of the container. The corresponding angular speed ω_* has to be determined numerically by the analysis presented in Sect. 2.

3.1 The liquid shape upon dewetting

For angular speeds $\omega > \omega_*$, the liquid withdraws from the bottom surface of the cylinder (5). On the microscopic scale, the withdrawal initially takes place by deposition of thin liquid film at the bottom of the cylinder. The film deposition will continue unless the centrifugal force is able to rupture the molecular liquid bonds within the film, beyond which the actual dewetting of the bottom of the cylinder could begin. The experimental

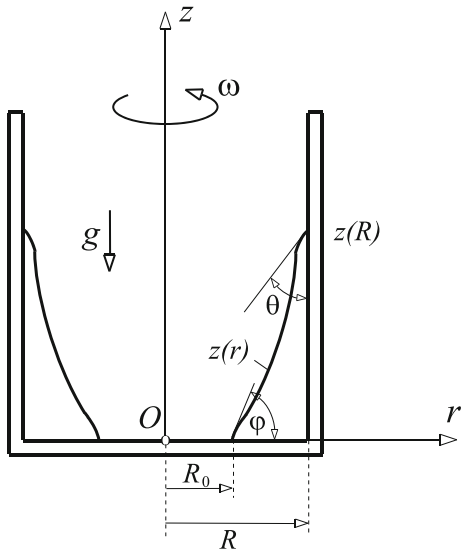

Fig. 5 The liquid surface shape after the onset of dewetting, which has spread to the radius R_0. The wetting contact angles at the *bottom* and the lateral wall of the cylinder are φ and θ, respectively

evidence for both possibilities has been reported in [37]. Let $R_0 < R$ denote the extent of deposited film or actual dewetting, as discussed above. Assuming again that the height of the cylindrical wall is large enough so that liquid does not spill over the side of the cylinder, the appropriate functional for the variational study is $\Pi = U - K - \lambda V$, where λ is the Lagrangian multiplier. The free energy, up to a constant term, is

$$U = 2\pi\sigma_{lv}S + 2\pi Rz(R)(\sigma_{sl} - \sigma_{sv}) + \pi R_0^2\sigma^* + 2\pi R_0\tau^* + \gamma_l \int_V \zeta \,\mathrm{d}V, \tag{3.2}$$

and $K = (\rho_l/2)\int_V \varrho^2 \mathrm{d}V$ is the kinetic energy of the liquid. The coordinates at an arbitrary point within the liquid are (ϱ, ζ). The governing equations in this section will be conveniently derived without the commitment to a particular choice of coordinates, so that the analysis encompasses the possibility that the function $r = r(z)$, rather than $z = z(r)$, is single-valued, which occurs in the case of hydrophobic bottom surface near the triple contact line. In the numerical evaluation, both cases can be treated simultaneously by taking the arc length s along the liquid/vapor interface as the parameter [38], so that $r = r(s)$ and $z = z(s)$.

In the case of actual dewetting, the surface energy σ^* in (3.2) is $\sigma^* = \hat{\sigma}_{sv} - \hat{\sigma}_{sl}$. For generality, it is assumed that the bottom surface of the container is different from the lateral wall surface, so that the surface energies at the bottom are $\hat{\sigma}_{sv}$ and $\hat{\sigma}_{sl}$, while the lateral wall has the surface energies σ_{sv} and σ_{sl}. Different surface energies can be a consequence of the manufacturing (deep drawing) production of the cylinder, or the bottom plate can be made of different material from the welded lateral wall of the cylinder. The line tension along the triple contact line at the bottom surface is τ^*, which is important in the early stages of dewetting, when $R_0 \ll R$ [39]. The line tension also includes the energy of the broken molecular bonds.

If the liquid withdraws from the bottom surface of the cylinder by leaving a thin film behind, the surface energy σ^* is equal to σ_{lv}. It is assumed that the film is sufficiently thick that its lower face, which is in contact with the solid, can still be assigned the surface energy σ_{sl}, while its upper face is assigned a surface energy σ_{lv} [40]. In this case $\tau^* = 0$, because the liquid elevates from the film smoothly and without contact with a solid surface of the cylinder.

If a surface element $\mathrm{d}S$ at an arbitrary point of S, which is not on the bounding circles $r = R_0$ or $r = R$, is given a virtual displacement δu, then $\delta(\mathrm{d}S) = -2\kappa\delta u_n \,\mathrm{d}S$, where δu_n is the projection of δu onto the surface outward normal. The surface elements at the points of the contact circles $r = R_0$ and $r = R$ need to be additionally stretched in the direction tangential to the surface, to preserve the liquid contact with the bottom of the cylinder and with its lateral wall, so that the total area change of the surface S can be written as

$$\delta S = -\int_S 2\kappa\delta u_n \,\mathrm{d}S - 2R_0\pi\cos\varphi\,\delta R_0 + 2R\pi\cos\theta\,\delta z(R). \tag{3.3}$$

Furthermore, by the Reynolds transport theorem,

$$\delta V = \int_S \delta u_n \, \mathrm{d}S, \quad \delta \int_V (\varrho^2, \zeta) \, \mathrm{d}V = \int_S (r^2, z) \, \delta u_n \, \mathrm{d}S. \tag{3.4}$$

Consequently, the variation of the potential function $\delta\Pi = \delta U - \delta K - \lambda \delta V$ becomes

$$\delta\Pi = -\int_S \left(2\sigma_{lv}\kappa - \gamma_l z + \frac{1}{2}\rho_l \omega^2 r^2 + \lambda\right) \delta u_n \, \mathrm{d}S + 2R\pi \, (\sigma_{sl} - \sigma_{sv} + \sigma_{lv}\cos\theta) \, \delta z(R)$$
$$+ 2R_0\pi \left(\sigma^* - \sigma_{lv}\cos\varphi + \frac{\tau^*}{R_0}\right) \delta R_0.$$

The stationary condition $\delta\Pi = 0$, defining a gyrostatic liquid shape, thus gives

$$2\sigma_{lv}\kappa - \gamma_l z + \frac{1}{2}\rho_l \omega^2 r^2 + \lambda = 0, \tag{3.5}$$

$$\sigma_{sl} - \sigma_{sv} + \sigma_{lv}\cos\theta = 0, \quad \sigma^* - \sigma_{lv}\cos\varphi + \frac{\tau^*}{R_0} = 0. \tag{3.6}$$

The last two expressions specify the wetting angles θ and φ as

$$\cos\theta = \frac{\sigma_{sv} - \sigma_{sl}}{\sigma_{lv}}, \quad \cos\varphi = \frac{\sigma^*}{\sigma_{lv}} + \frac{\tau^*}{R_0\sigma_{lv}}. \tag{3.7.1,2}$$

Equation (3.7.1) is Young's equation for the contact angle θ between the liquid and the vertical wall. Equation (3.7.2) defines the contact angle φ between the liquid and the bottom of the cylinder. The sign in front of the line tension (τ^*) term is opposite to the (minus) sign appearing in the corresponding equation for the contact angle of a liquid drop deposited on a solid substrate [41], because the center of curvature of the triple contact line is at the center of dewetted island in the present case, while it is at the center of the solid/liquid interface in the case of a drop. If a thin film is deposited behind a withdrawing liquid, then $\sigma^* = \sigma_{lv}$ and $\tau^* = 0$, so that (3.7) gives $\varphi = 0$, that is, the liquid elevates from a deposited film with a vanishing slope, $z'(R_0) = 0$. The volume of the deposited thin film is assumed to be negligibly small relative to the entire volume of the rotating liquid.

3.2 Determination of the Lagrangian multiplier

Consider the liquid shape described by a single-valued function $z = z(r)$, which physically applies if the bottom surface is hydrophilic ($\varphi \le \pi/2$), or if a thin film is deposited behind a withdrawing liquid ($\varphi = 0$). In view of the identity (2.22), the differential Eq. (3.5) can be rewritten as

$$\frac{\mathrm{d}}{\mathrm{d}r}\left[\frac{rz'}{(1+z'^2)^{1/2}}\right] = \frac{\gamma_l}{\sigma_{lv}}\left(rz - \frac{\omega^2}{2g}r^3\right) + \frac{\lambda}{\sigma_{lv}}r. \tag{3.8}$$

Upon the integration from R_0 to R, there follows

$$\lambda = \frac{2\sigma_{lv}}{R^2 - R_0^2}(R\cos\theta - R_0\sin\varphi) - \gamma_l\left[\frac{V}{\pi(R^2 - R_0^2)} - \frac{\omega^2}{4g}(R^2 + R_0^2)\right]. \tag{3.9}$$

When (3.9) is substituted back into (3.5), the differential equation for the liquid surface becomes

$$\frac{z''}{(1+z'^2)^{3/2}} + \frac{z'}{r(1+z'^2)^{1/2}} - \frac{\gamma_l}{\sigma_{lv}}z = q(r), \tag{3.10}$$

$$q(r) = \frac{2}{R^2 - R_0^2}(R\cos\theta - R_0\sin\varphi) - \frac{\gamma_l}{\sigma_{lv}}\left[\frac{V}{\pi(R^2 - R_0^2)} - \frac{\omega^2}{4g}(R^2 + R_0^2 - 2r^2)\right]. \tag{3.11}$$

The accompanying boundary conditions are $z'(R_0) = \tan\varphi$, $z'(R) = \cot\theta$, where the contact angles φ and θ are specified by (3.7.1,2). In addition, $z(R_0) = 0$, by the definition of R_0.

3.3 Uniqueness and stability

We did not construct the uniqueness and stability proves for the gyrostatic liquid shape upon the onset of dewetting at the bottom of the cylindrical container. Numerical evaluations, however, suggest that, among all axisymmetric shapes, the determined gyrostatic shape corresponding to a selected set of control parameters is unique and stable. Non-axisymmetric bifurcations of axisymmetric gyrostatic configurations were not studied, but may be unlikely because of the stabilizing effect of the constraining lateral wall and the downward direction of gravity (toward the bottom of the cylindrical container). It is energetically and topologically challenging for the liquid to find a non-axisymmetric gyrostatic shape in an axisymmetric circular cylinder, wetting its wall with the same contact angle all around an asymmetric triple contact line. This, however, has to be verified, and thus, the extension of the present work to examine the stability of axisymmetric gyrostatic shape with respect to non-axisymmetric perturbations is a worthwhile goal for future research.

3.4 Iterative numerical integration of the differential equation

The solution of the non-linear differential Eq. (3.10) proceeds numerically in an iterative semi-inverse manner. For a given $\omega > \omega_*$, one assumes the value of the radius R_0 and solves (3.10), subjected to the boundary conditions $z(R_0) = 0$ and $z'(R_0) = \tan\varphi$. If the resulting slope $z'(R) \neq \cot\theta$, the initial guess for R_0 is modified, and the procedure repeated until the boundary condition $z'(R) = \cot\theta$ is numerically satisfied. There is only one such shape corresponding to a given volume of the liquid.

The numerical evaluation is facilitated by rewriting (3.10) and (3.11) in the non-dimensional form

$$\frac{\bar{z}''}{(1+\bar{z}'^2)^{3/2}} + \frac{\bar{z}'}{\bar{r}(1+\bar{z}'^2)^{1/2}} - Bo\,\bar{z} = \bar{q}(r), \tag{3.12}$$

$$q(r) = \frac{2}{1-\bar{R}_0^2}(\cos\theta - \bar{R}_0\sin\varphi) - Bo\left[\frac{\bar{V}}{1-\bar{R}_0^2} - \frac{\eta}{4}(1+\bar{R}_0^2 - 2\bar{r}^2)\right]. \tag{3.13}$$

Figure 6a, b shows the liquid shape in the case $Bo = 2$ and $\eta = 5$, when the wetting contact angles are $(\theta = 45°, \varphi = 45°)$ and $(\theta = 135°, \varphi = 45°)$. Figure 6c, d shows the same when $\varphi = 0$. The normalized volume of the liquid was $\bar{V} \approx 0.1288$. For hydrophobic surface of the cylinder wall, the extent of dewetting, as well as the rotation-induced rising of the liquid, is suppressed relative to the hydrophilic surfaces. The dashed curves specify the liquid shape in the case when the surface tension effects are absent.

4 Liquid shape in a rotating cylinder under zero gravity

The surface tension plays an increasingly important role under conditions of reduced gravity [10,12]. Such studies are of importance for better understanding of the fluid behavior in the projectile and spacecraft fuel tanks and for preventing flight instabilities due to fluid-tank interactions.

4.1 Determination of the liquid shape before dewetting

If the surface tension is ignored ($\sigma_{lv} = 0$), the liquid in the container cannot sustain rotation in the zero gravity field. Indeed, the expressions for the liquid pressure at point C, calculated from either the pressure at point A or B (Fig. 7a), are

$$p_C = p_A + \frac{1}{2}\rho_l r^2\omega^2, \qquad p_C = p_B. \tag{4.1}$$

Since $p_A = p_B = p_0$, the above two expressions for p_C are irreconcilable, and thus, there is no gyrostatic configuration, unless $\omega = 0$.

In the absence of gravity, Eq. (2.26) reduces to

$$\frac{z''}{(1+z'^2)^{3/2}} + \frac{z'}{r(1+z'^2)^{1/2}} = \frac{2\cos\theta}{R} + \frac{\rho_l\omega^2}{4\sigma_{lv}}(R^2 - 2r^2), \tag{4.2}$$

while Eq. (2.25) becomes

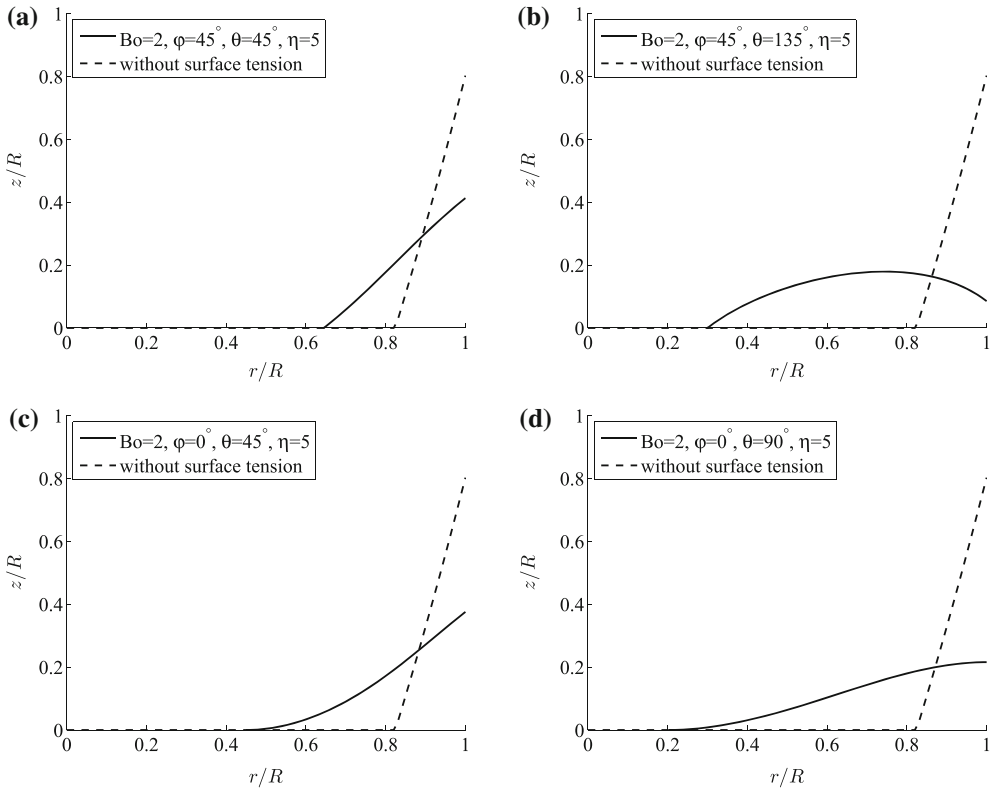

Fig. 6 The shape of the liquid surface, corresponding to the indicated values of B, η, φ, and θ. The normalized liquid volume is $\bar{V} \approx 0.1288$. Without the surface effects, $\bar{R}_0 = 0.824$ and $\bar{z}(R) = 0.8025$. With the surface effects: **a** $\bar{R}_0 = 0.6451$ and $\bar{z}(R) = 0.4127$. **b** $\bar{R}_0 = 0.3$ and $\bar{z}(R) = 0.0851$. **c** $\bar{R}_0 = 0.4518$ and $\bar{z}(R) = 0.3755$. **d** $\bar{R}_0 = 0.2052$ and $\bar{z}(R) = 0.2157$

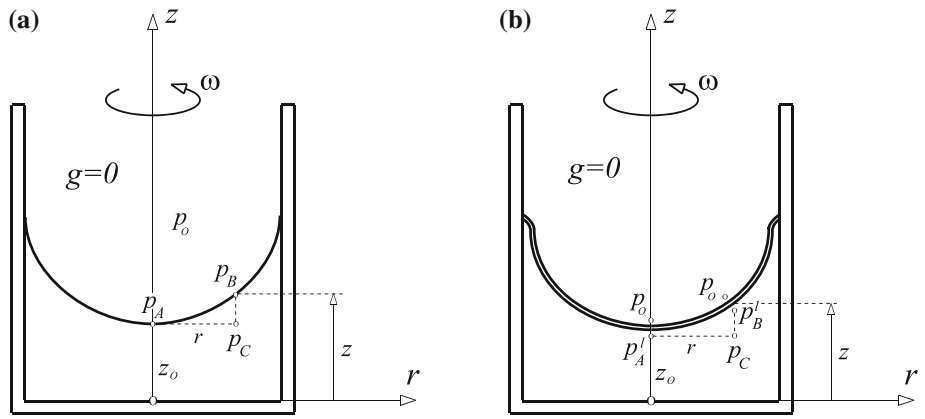

Fig. 7 **a** In the absence of surface tension, the expressions for liquid pressure at point C, calculated from the pressures at points A and B, are irreconcilable. **b** In the presence of surface tension, the liquid surface finds an equilibrium shape. The liquid pressure at point C can be calculated from the liquid pressures at points A and B, while the pressure jumps across the liquid/vapor interface at those points can be expressed in terms of the corresponding local curvatures

$$\kappa(0) = \frac{\cos\theta}{R} + \frac{\rho_l \omega^2}{8\sigma_{lv}} R^2. \tag{4.3}$$

The differential Eq. (4.2) allows a closed-form solution. Indeed, by rewriting (4.2) as

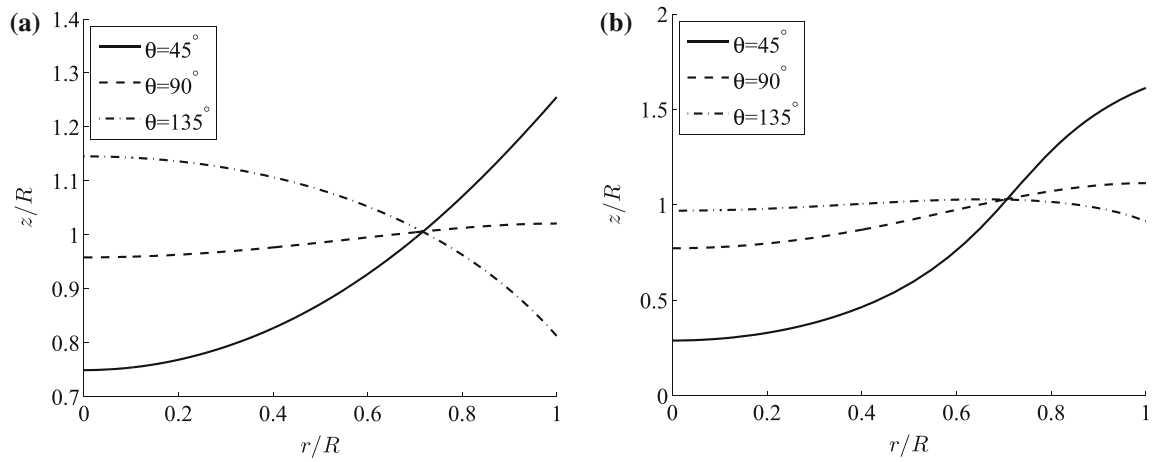

Fig. 8 **a** $B_\omega = 2$. *Solid*: $\bar{z}(0) = 0.7492$ and $\bar{z}(R) = 1.2553$. *Dashed*: $\bar{z}(0) = 0.9582$ and $\bar{z}(R) = 1.0209$. *Dotted-dashed*: $\bar{z}(0) = 1.1454$ and $\bar{z}(R) = 0.8124$. **b** $B_\omega = 10$. *Solid*: $\bar{z}(0) = 0.2892$ and $\bar{z}(R) = 1.6125$. *Dashed*: $\bar{z}(0) = 0.7727$ and $\bar{z}(R) = 1.1137$. *Dotted-dashed*: $\bar{z}(0) = 0.9695$ and $\bar{z}(R) = 0.9138$. The normalized volume $\bar{V} = 1$

$$\frac{\mathrm{d}}{\mathrm{d}r}\left[\frac{rz'}{(1+z'^2)^{1/2}}\right] = 2\kappa(0)r - \frac{\rho_l}{2\sigma_{lv}}\omega^2 r^3, \tag{4.4}$$

integration gives

$$\frac{z'}{(1+z'^2)^{1/2}} = \kappa(0)r - \frac{\rho_l}{8\sigma_{lv}}\omega^2 r^3. \tag{4.5}$$

The integration constant vanishes, because $z'(0) = 0$. The solution of this equation is

$$z = z(0) + \int_0^r \frac{t(\varrho)\,\mathrm{d}\varrho}{[1-t^2(\varrho)]^{1/2}}, \quad t(\varrho) = \kappa(0)\varrho - \frac{\rho_l}{8\sigma_{lv}}\omega^2\varrho^3. \tag{4.6}$$

The elevation $z(0)$ is obtained a posteriori, by using (4.6) to evaluate the liquid volume from $V = 2\pi\int_0^R rz\,\mathrm{d}r$. This gives

$$z(0) = \frac{1}{\pi R^2}\left\{V - 2\pi\int_0^R r\,\mathrm{d}r\int_0^r \frac{t(\varrho)\,\mathrm{d}\varrho}{[1-t^2(\varrho)]^{1/2}}\right\}. \tag{4.7}$$

Among all neighboring configurations, the so-determined equilibrium configuration is unique and stable, as shown for $g \geq 0$ in Sect. 2.

4.1.1 Numerical evaluations

By using the rotation-induced Bond number (2.31), the curvature $\kappa(0)$ in (4.3), and $t(\varrho)$ in Eq. (4.6), can be expressed as

$$\kappa(0) = \frac{1}{R}\left(\cos\theta + \frac{1}{8}B_\omega\right), \quad t(\varrho) = \left\{\cos\theta + \frac{B_\omega}{8}\left[1 - \left(\frac{\varrho}{R}\right)^2\right]\right\}\left(\frac{\varrho}{R}\right). \tag{4.8}$$

Figure 8a shows the liquid shape for three indicated values of the contact angle θ, in the case $B_\omega = 2$. Figure 8b shows the same in the case $B_\omega = 10$. The curves intersect at one point coincidentally, because the contact angles $\theta = 45°$ and $\theta = 135°$ are at $\mp 45°$ relative to the contact angle $\theta = 90°$.

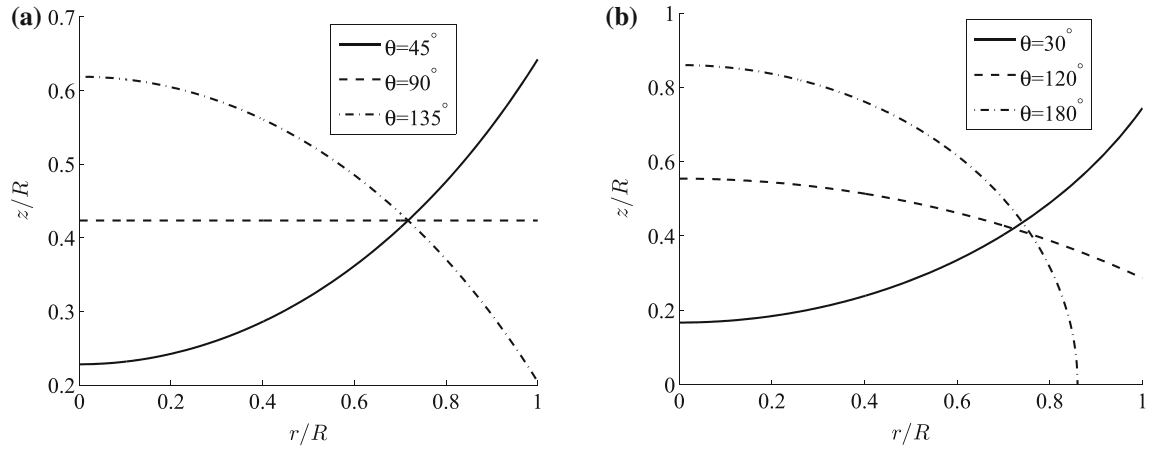

Fig. 9 Obtained from (4.6) with $B_\omega = 0$, or (4.9) and (4.10). **a** Volume $\bar{V} = 0.4235$. *Solid*: $\bar{z}(0) = 0.2282$ and $\bar{z}(R) = 0.6424$. *Dashed*: $\bar{z}(0) = \bar{z}(R) = 0.4325$. *Dotted-dashed*: $\bar{z}(0) = 0.6188$ and $\bar{z}(R) = 0.2046$. **b** Volume $\bar{V} = 0.42351$. *Solid*: $\bar{z}(0) = 0.1669$ and $\bar{z}(R) = 0.7443$. *Dashed*: $\bar{z}(0) = 0.5543$ and $\bar{z}(R) = 0.2864$. *Dotted-dashed*: semi-spherical shape of radius $\bar{z}(0) = 0.8596$, if $\varphi = 90°$

4.1.2 Stationary cylinder

If $\omega = 0$, the curvature of the liquid surface is constant and equal to $\kappa(0) = \cos\theta/R$. The shape of the surface is explicitly specified by (4.6), which gives

$$z = z(0) + \frac{R}{\cos\theta}\left[1 - \left(1 - \frac{r^2}{R^2}\cos^2\theta\right)^{1/2}\right]. \tag{4.9}$$

This represents a sphere of radius $R/\cos\theta$, centered at the point with the coordinates $r = 0$ and $z = z(0) + R/\cos\theta$. The elevation $z(0)$ is, from (4.7),

$$z(0) = h - \frac{R}{3\cos\theta}\,\frac{(1-\sin\theta)(1+2\sin\theta)}{1+\sin\theta}. \tag{4.10}$$

Finn [30,31] has shown that the equilibrium liquid shape in a vertical cylindrical container, with the gravity (however, small) directed downwards, and with constant contact angle between the liquid and the cylinder, is unique and stable with respect to both axisymmetric and non-axisymmetric perturbations of its shape.[2] This also follows from our analysis in Sect. 2.2.

Figure 9 shows the liquid shape in a stationary cylinder for six different values of the contact angle θ, when $\bar{V} = 0.4325$. In the case of a super-hydrophobic surface of the wall ($\theta = 180°$), the liquid does not touch the wall, but forms either a semi-spherical drop of radius $0.8596R$, if the wetting contact angle of the bottom surface is $\varphi = 90°$, or a spherical drop of radius $0.6823R$, if the wetting contact angle of the bottom surface is $\varphi = 180°$.

4.2 Determination of the liquid shape upon dewetting

The liquid surface will touch the bottom of the cylinder if $z(0) = 0$ in (4.7), which yields

$$h = \frac{2}{R^2}\int_0^R r\,\mathrm{d}r \int_0^r \frac{t(\varrho)\,\mathrm{d}\varrho}{[1-t^2(\varrho)]^{1/2}}. \tag{4.11}$$

[2] Note, however, that in the absence of gravity, the equilibrium liquid shape is unstable to at least some infinitesimal perturbation of the boundary shape of the cylinder, for which there is no solution for the capillary surface at all; [30], page 138.

In view of the expression for $t(\varrho)$ in (4.6), Eq. (4.11) specifies the angular speed ω_* at the onset of dewetting. The objective of this Section is to determine the shape of the liquid for $\omega > \omega_*$. In the absence of gravity, Eq. (3.10) becomes

$$\frac{z''}{(1+z'^2)^{3/2}} + \frac{z'}{r(1+z'^2)^{1/2}} = \frac{2}{R^2 - R_0^2}(R\cos\theta - R_0\sin\varphi) + \frac{\rho_l\omega^2}{4\sigma_{lv}}(R^2 + R_0^2 - 2r^2).$$

By rewriting the above as

$$\frac{\mathrm{d}}{\mathrm{d}r}\left[\frac{rz'}{(1+z'^2)^{1/2}}\right] = \frac{2r}{R^2 - R_0^2}(R\cos\theta - R_0\sin\varphi) + \frac{\rho_l\omega^2}{4\sigma_{lv}}[(R^2 + R_0^2)r - 2r^3], \tag{4.12}$$

the integration from R_0 to R gives

$$\frac{z'}{(1+z'^2)^{1/2}} = t(r), \tag{4.13}$$

where

$$t(r) = \frac{1}{R^2 - R_0^2}\frac{1}{r}\left[(r^2 - R_0^2)R\cos\theta + (R^2 - r^2)R_0\sin\varphi\right] + \frac{\rho_l\omega^2}{8\sigma_{lv}}\frac{1}{r}(R^2 - r^2)(r^2 - R_0^2).$$

The solution of (4.13) is

$$z = \int_{R_0}^{r} \frac{t(\varrho)\,\mathrm{d}\varrho}{[1 - t^2(\varrho)]^{1/2}}. \tag{4.14}$$

4.2.1 Iterative numerical integration

Since the radius R_0 is not known in advance, the solution of the problem proceeds iteratively. For a given $\omega > \omega_*$, the radius R_0 is assumed and the corresponding shape $z = z(r)$ evaluated from (4.14). The volume of the liquid is then calculated from

$$V = 2\pi \int_{R_0}^{R} r\,\mathrm{d}r \int_{R_0}^{r} \frac{t(\varrho)\,\mathrm{d}\varrho}{[1 - t^2(\varrho)]^{1/2}}. \tag{4.15}$$

If the so-calculated volume is different from the actual volume of the liquid, the new value of R_0 is selected, and the procedure repeated until the calculated volume is equal to the actual liquid volume. In the case of a stationary cylinder, the iterative procedure is still needed, except that the function $t(r)$ is simplified by the specification $\omega = 0$.

Figure 10a, b shows the liquid shape for three selected values of the contact angle θ, in the case when the dewetting contact angle at the bottom surface of the cylinder is (a) $\varphi = 45°$, and (b) $\varphi = 90°$. In all cases, the volume of the liquid was $\bar{V} = 0.1794$, and the rotation-induced Bond number was $B_\omega = 20$. Figure 10c shows the liquid shape for three selected values of dewetting contact angle φ, and the same contact angle $\theta = 45°$. Finally, Fig. 10d shows the results when the contact angles at the bottom surface and the surface of the lateral wall are equal to each other ($\varphi = \theta$). The plots demonstrate that the hydrophobicity of the surface of the lateral wall suppresses lifting of the liquid at the circumference $r = R$, while the increase of dewetting contact angle at the bottom surface of the cylinder intensifies the extent of dewetting. If the cylinder was closed at the top, the liquid would wet the roof and, at a sufficiently high angular speed, take the shape of an annular cylinder, except near the triple contact edges, where the surface tensions intervene to fulfill Young's condition for the contact angle. An analysis of a bubble zone below the ceiling of a closed cylinder, expanding toward its floor, has been presented in [14], with further discussion and reference to other work given in [4].

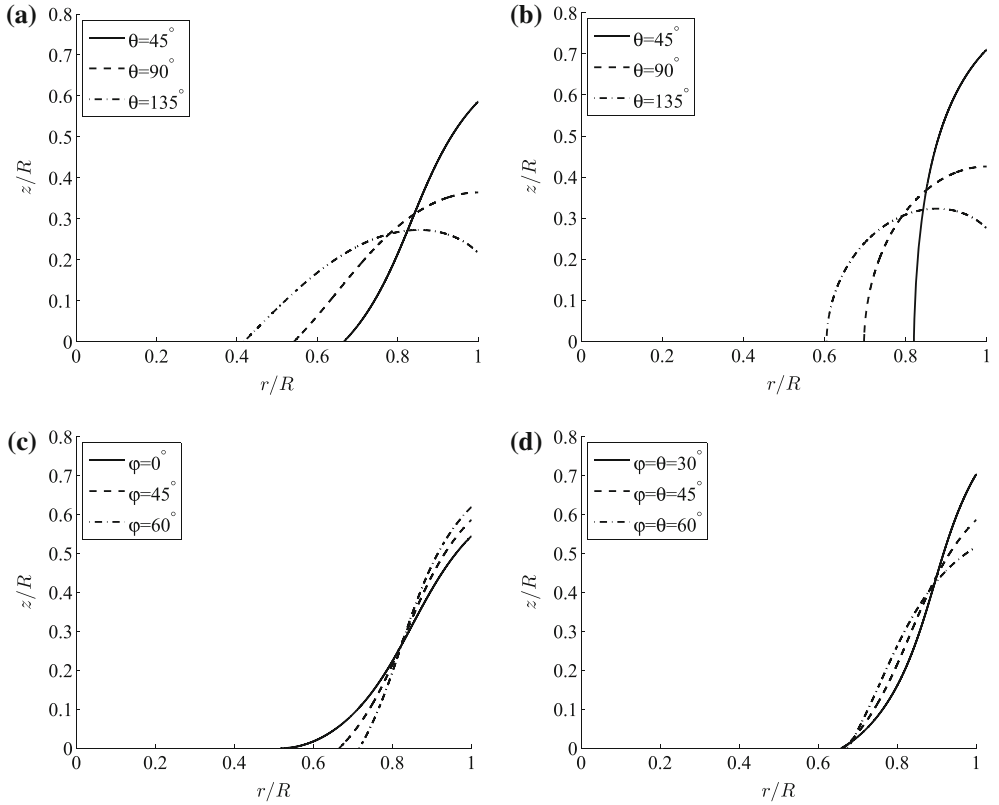

Fig. 10 The shape of the liquid surface corresponding to $B_\omega = 20$ and $\bar{V} \approx 0.1749$. **a** The angle $\varphi = 45°$. *Solid*: $\bar{R}_0 = 0.6659$ and $\bar{z}(R) = 0.5860$. *Dashed*: $\bar{R}_0 = 0.5419$ and $\bar{z}(R) = 0.3643$. *Dotted-dashed*: $\bar{R}_0 = 0.4178$ and $\bar{z}(R) = 0.2166$. **b** The angle $\varphi = 90°$. *Solid*: $\bar{R}_0 = 0.8207$ and $\bar{z}(R) = 0.7102$. *Dashed*: $\bar{R}_0 = 0.6979$ and $\bar{z}(R) = 0.4257$. *Dotted-dashed*: $\bar{R}_0 = 0.6053$ and $\bar{z}(R) = 0.2750$. **c** The angle $\theta = 45°$. *Solid*: $\bar{R}_0 = 0.5192$ and $\bar{z}(R) = 0.5441$. *Dashed*: $\bar{R}_0 = 0.6659$ and $\bar{z}(R) = 0.5860$. *Dotted-dashed*: $\bar{R}_0 = 0.7167$ and $\bar{z}(R) = 0.6189$. **d** *Solid*: $\bar{R}_0 = 0.6593$ and $\bar{z}(R) = 0.7071$. *Dashed*: $\bar{R}_0 = 0.6659$ and $\bar{z}(R) = 0.5860$. *Dotted-dashed*: $\bar{R}_0 = 0.6752$ and $\bar{z}(R) = 0.5162$

5 Conclusions

We presented in this paper an analysis of axisymmetric gyrostatic shape of liquid in a uniformly rotating cylinder in the presence of surface tension. The analysis is based on the variational approach, with an effective mechanical potential used as a functional, subjected to the constraint of liquid incompressibility. This yields the governing Young–Laplace's differential equation for the shape of the liquid surface, and the expressions for the contact angle between the liquid and the lateral wall of the cylinder. The macroscopic contact angle is shown to be independent of gravity and the angular speed of rotation and given by Young's, or modified Young's, equation. For a given angular momentum, the determined axisymmetric shape of liquid surface is unique and stable, because it corresponds to the minimum of everywhere convex potential functional in the space of all functions defining the shape of liquid surface before the onset of dewetting. For sufficiently high angular velocity, the liquid surface dewets the bottom of the cylinder. Two scenarios of liquid withdrawal from the bottom are considered, with and without deposition of thin film. The corresponding potential functional is constructed and used to derive the governing differential equation for the liquid shape, and the expressions for the wetting angles at the lateral wall and the bottom of the cylinder. The axisymmetric gyrostatic shape of liquid surface is determined for cylinders whose radii are comparable to the capillary length of liquid in the gravitational or reduced gravitational field. The differential equations are solved numerically by an iterative procedure similar to the well-known procedure used to determine the equilibrium shape of a sessile or pendant drop in the gravitational field. The capillary effects are found to be particularly pronounced for hydrophobic surfaces, which oppose the rotation-induced lifting of the liquid. The increase of dewetting contact angle intensifies dewetting at the bottom surface of the cylinder. The liquid shape is then analyzed under the zero gravity conditions. A closed-form solution is obtained in the rotation range before the onset of dewetting.

An iterative scheme is applied to determine the liquid shape after the onset of dewetting. A variety of shapes, corresponding to different wetting angles and speeds of rotation, are calculated and discussed. The extension of the present study to examine the stability of axisymmetric gyrostatic shape of liquid surface, after the onset of dewetting at the bottom of the cylinder, with respect to non-axisymmetric perturbations of its shape is a worthwhile goal of future research.

Acknowledgments This research was supported by the Montenegrin Academy of Sciences and Arts and the MAE endowment fund at UCSD. Discussions with professor Frank E. Talke and valuable comments and suggestions by reviewers are gratefully acknowledged.

Appendix: Liquid shape in the absence of surface tension

If the surface tension is not included in the analysis, so that there is no interface layer between the liquid and gas, there is no jump in pressure across the surface S, so that $\Delta p(r) = 0$. The well-known parabolic shape of the liquid surface is then [42]

$$z(r) = h + \frac{R^2\omega^2}{4g}\left(2\,\frac{r^2}{R^2} - 1\right). \tag{A.1}$$

In particular, $z(R) - h = h - z(0) = R^2\omega^2/(4g)$, so that the lowering of the liquid at the center is the same as its rising at the edge.

In order that there is no dewetting at the bottom of the cylinder, $z(0) \geq 0$ (with the origin at the bottom of the cylinder), the angular speed must be such that $\omega^2 \leq 4gh/R^2$. In order that liquid does not spill over the side of the cylinder, $z(R) \leq H$, the angular speed must satisfy the condition $\omega^2 \leq 4g(H-h)/R^2$. Thus,

$$\omega^2 \leq \frac{4g}{R^2}\begin{cases} H-h, & h < H \leq 2h, \\ h, & H \geq 2h. \end{cases} \tag{A.2}$$

The contact angle is obtained from the expression $z'(R) = \cot\theta$, which gives

$$\tan\theta = \frac{1}{\eta}, \quad \cos\theta = \frac{\eta}{(1+\eta^2)^{1/2}}, \quad \eta = \frac{R\omega^2}{g}. \tag{A.3}$$

The contact angle θ decreases with the increasing ω, and it also depends on g and R, in contrast to the analysis which includes the surface tension, where the contact angle is constant (independent of ω, R, and g), and given by Young's Eq. (2.17), in terms of the surface tensions alone.

If $H > 2h$ and $\omega > \omega_1 = 2\sqrt{gh}/R$, the portion of the bottom of the container will be dewetted. Implicit assumption is that the centrifugal force is strong enough to break the bonds holding the liquid molecules together at the bottom of the cylinder. If dewetting extends to the radius $0 \leq R_0 \leq R$, the liquid surface has the profile

$$z(r) = \frac{\omega^2}{2g}(r^2 - R_0^2), \quad \omega^2 = \omega_1^2\left(1 - \frac{R_0^2}{R^2}\right)^{-2}, \quad (R_0 \leq r \leq R). \tag{A.4}$$

In order that liquid does not spill over the side of the cylinder, the radius of the dewetting region is bounded by

$$R_0 \leq R\left(1 - 2\,\frac{h}{H}\right)^{1/2}, \quad H > 2h. \tag{A.5}$$

The contact angles at the bottom of the cylinder and the lateral wall are

$$\tan\varphi = \eta_0 = \frac{R_0\omega^2}{g}, \quad \tan\theta = \frac{1}{\eta} = \frac{g}{R\omega^2}. \tag{A.6}$$

References

1. Greenspan, H.P.: The Theory of Rotating Fluids. Cambridge University Press, Cambridge (1980)
2. Myshkis, A.D., Babskii, V.G., Kopachevskii, N.D., Slobozhanin, L.A., Tyuptsov, A.D.: Low-gravity Fluid Mechanics. Mathematical Theory of Capillary Phenomena. Springer-Verlag, Berlin (1987). Translated from Russian edition: Gidromekhanika nevesomosti. Nauka, Moscow (1976)
3. Langbein, D.: Capillary Surfaces. Shape–Stability–Dynamics, in Particular Under Weightlessness. Springer Tracts in Modern Physics **178**. Springer, Berlin (2002)
4. Ibrahim, R.A.: Liquid Sloshing Dynamics. Theory and Applications. Cambridge University Press, Cambridge (2005)
5. Turkington, R.R., Osborne, D.V.: On the influence of surface tension on the surfcae profile of a rotating liquid. Proc. Phys. Soc. **82**, 614–619 (1963)
6. Radoev, R.: On a possibility of surface tension measurement via rotating meniscus. Ann. Univ. Sofia–Fac. Chim. **61**, 361–366 (1966/67)
7. Ogorelec, Z.: On the shape of a rotating liquid surface. Eur. J. Phys. **18**, 256–259 (1995)
8. Wasserman, M.L., Slattery, J.C.: The surface profile of a rotating liquid. Proc. Phys. Soc. **84**, 795–802 (1964)
9. Aronson, M.P., Princen, H.M.: Shape of a meniscus in a rotating vertical tube. J. Chem. Soc. Faraday Trans. 1 Phys. Chem. Condens. Phases **74**, 555–574 (1978)
10. Slobozhanian, L.A.: Hydrostatics in weak force fields. Equilibrium shapes of the surface of a rotating liquid under zero-g. Fluid Dynamics **1**, 113–116 (1966). Translated from Russian: Izv. Ak. Nauk SSSR, Mekh. Zhidkosti i Gaza **1**, 157–160 (1966)
11. Wichterle, K., Wichterle, O.: Surface shapes of fluids in rotating vessels. Appl. Sci. Res. **22**, 150–158 (1970)
12. Bauer, H.F.: Rotating finite liquid systems under zero gravity. Forsch. Ingenieurwes. **48**, 159–179 (1982)
13. Leslie, F.: Measurements of rotating bubble shapes in a low-gravity environment. J. Fluid Mech. **161**, 269–279 (1985)
14. Hung, R.J., Tsao, Y.D., Hong, B.B., Leslie, F.W.: Dynamics of surface tension in microgravity environment. Progress Aeronaut. Astronaut. **127**, 124–150 (1990)
15. Brown, R.A., Scriven, L.E.: The shapes and stability of captive rotating drops. Phil. Trans. Roy. Soc. Lond. **297**, 51–79 (1980)
16. Benner, R.E. Jr.., Basaran, O.A., Scriven, L.E.: Equilibria, stability and bifurcations of rotating columns of fluid subjected to planar disturbances. Proc. R. Soc. Lond. A **433**, 81–99 (1991)
17. Boadi, D.K., Marmur, A.: Equilibrium of a liquid in a rotating groove. Chem Eng. Sci. **47**, 4287–4294 (1992)
18. Kruse, H.P., Mahalov, A., Marsden, J.E.: On the Hamiltonian structure and three-dimensional instabilities of rotating liquid bridges. Fluid Dyn. Res. **24**, 37–59 (1999)
19. Haas, A., Pollak, T., Aksel, N.: Side wall effects in thin gravity-driven film flow—steady and draining flow. Phys. Fluids **23**, 062107-1–11 (2011)
20. Pollak, T., Haas, A., Aksel, N.: Side wall effects on the instability of thin gravity-driven films-From long-wave to short-wave instability. Phys. Fluids **23**, 094110-1–7 (2011)
21. Stewartson, K.: On almost rigid rotations. J. Fluid Mech. **2**, 17–26 (1957)
22. Miles, J.W.: Free-surface oscillations in a slowly rotating liquid. J. Fluid Mech. **17**, 187–194 (1963)
23. Greenspan, H.P., Howard, L.N.: On a time-dependent motion of a rotating fluid. J. Fluid Mech. **17**, 385–404 (1963)
24. Neitzel, G.P., Davis, S.H.: Centrifugal instabilities during spin-down to rest in finite cylinders. Numer. Exp. J. Fluid Mech. **102**, 329–352 (1981)
25. Bormashenko, E., Whyman, G.: Variational approach to wetting problems: calculation of a shape of sessile liquid drop deposited on a solid substrate in external field. Chem. Phys. Lett. **463**, 103–105 (2008)
26. Lubarda, V.A., Talke, K.A.: Configurational forces and shape of a sessile droplet on a rotating solid substrate. Theor. Appl. Mech. **39**, 27–54 (2012)
27. Gennes, P.G.de : Wetting: statics and dynamics. Rev. Modern Phys. **57**, 827–863 (1985)
28. Blokhuis, E.M., Shilkrot, Y., Widom, B.: Young's law with gravity. Mol. Phys. **86**, 891–899 (1995)
29. Lubarda, V.A.: Mechanics of a liquid drop deposited on a solid substrate. Soft Matter **8**, 10288–10297 (2012)
30. Finn, R.: Equilibrium capillary surfaces. Springer, New York (1986)
31. Finn, R.: Non uniqueness and uniqueness of capillary surfaces. Manuscripta Math. **61**, 347–372 (1988)
32. Bashforth, F., Adams, J.C.: An Attempt to Test the Theory of Capillary Action. Cambridge University Press, Cambridge (1983)
33. Padday, J.F.: Theory of surface tension. In: Matijevic, E. (ed.) Surface and Colloid Science, vol. 1 , pp. 101–151. Wiley, New York (1969)
34. Padday, J.F.: Capillary in microgravity. In: Pétré, G., Sanfeld, A. (eds.) Capillarity Today. Lecture Notes in Physics, vol. 386, pp. 90–107. Springer, New York (1991)
35. Blokhuis, E.M.: Liquid drops at surfaces. In: Hartland, S. (ed.) Surface and Interfacial Tension: Measurement, Theory, and Applications, Surfactant Science Series, vol. 119, pp. 147–193. Marcel Dekker, Inc., New York (2005)
36. Li, D., Cheng, P., Neumann, A.W.: Contact angle measurement by axisymmetric drop shape analysis (ADSA). Adv. Coll. Interface Sci. **39**, 347–382 (1992)
37. Mukhopadhyay, S., Behringer, R.: Wetting dynamics of thin liquid films and drops under Marangoni and centrifugal forces. J. Phys. Condens. Matter **21**, 464123-1–9 (2009)
38. Slobozhanin, L.A., Alexander, J.I.D., Fedoseyev, A.I.: Shape and stability of doubly connected axisymmetric free surfaces in a cylindrical container. Phys. Fluids **11**, 3668–3677 (1999)
39. Widom, B.: Line tension and the shape of a sessile drop. J. Phys. Chem. **99**, 2803–2806 (1995)
40. Gennes, P.G.de , Brochard-Wyart, F., Quéré, D.: Capillarity and Wetting Phenomena. Springer, Berlin (2004)
41. Lubarda, V.A., Talke, K.A.: Analysis of the equilibrium droplet shape based on an ellipsoidal droplet model. Langmuir **27**, 10705–10713 (2011)
42. White, F.M.: Fluid Mechanics, 6th ed.. McGraw-Hill, New York (2008)